PFC/JA-82-33

Cross-field Free Electron Laser Instability for a Tenuous Electron Beam

Ronald C. Davidson and Wayne A. McMullin
Plasma Fusion Center, Massachusetts Institute of Technology,
Cambridge, MA 02139

Kang Tsang
Plasma Research Institute, Science Applications Inc.
Boulder, Colorado 80302

PFC/JA 82-33

Cross-field free electron laser instability for a tenuous electron beam

Ronald C. Davidson and Wayne A. McMullin
Plasma Fusion Center, Massachusetts Institute of Technology, Cambridge, Massachusetts 02139
Kang Tsang
Plasma Research Institute, Science Applications Inc., Boulder, Colorado 80302

(Received 8 December 1982; accepted 15 September 1983)

The free electron laser instability is investigated for a tenuous circulating electron beam propagating perpendicular to a uniform magnetic field $B_0\hat{e}_z$ and transverse wiggler field modeled by $B_w \sin k_0 y \hat{e}_x$ in planar geometry. Unlike the rippled-field magnetron which operates at Brillouin flow, the present analysis assumes a low-density electron beam with $\omega_p^2 \ll \Omega_c^2$. Making use of a macroscopic cold-fluid model for the electrons coupled with Maxwell's equations for the fields, it is found that wave perturbations with ordinary-mode polarization ($\delta \mathbf{E} \| \mathbf{B}_0$ and $\delta \mathbf{B} \perp \mathbf{B}_0$) amplify with characteristic maximum growth rate $\mathrm{Im}(\delta\omega) = \omega_p(\Omega_w/2\sqrt{2}ck_0)$ and emission frequency $\omega_r = (1+\beta_E)\gamma_E^2 k_0 V_E$. Here, $\Omega_w = eB_w/\gamma_E mc$, $\beta_E = V_E/C$, $\gamma_E = (1-\beta_E^2)^{-1/2}$, and $V_E = -cE_0/B_0$, where E_0 is the applied electric field across the anode–cathode gap. Depending on the size of Ω_w/ck_0, the characteristic exponentiation time $\omega_p^{-1}(\Omega_w/2\sqrt{2}ck_0)^{-1}$ for the cross-field free electron laser instability can be relatively short in units of ω_p^{-1}.

I. INTRODUCTION AND SUMMARY

There have been several theoretical[1–12] and experimental[13–20] studies of free electron lasers in linear (straight) geometry with transverse[1–8] or longitudinal[9–12] wiggler magnetic fields. Such configurations have gain limitations imposed by the finite length of the interaction region. In the present analysis, we consider the free electron laser (FEL) instability for a tenuous circulating electron beam propagating perpendicular to a uniform magnetic field $B_0\hat{e}_z$ and transverse wiggler field $B_w \sin k_0 y \hat{e}_x$ (Fig. 1), where $\lambda_0 = 2\pi/k_0$ is the wiggler wavelength and $B_w = \text{const}$ is the wiggler amplitude. The planar configuration in Fig. 1(a) is used to model the cylindrical geometry in Fig. 1(b) in the limit of large aspect ratio $R_0 \gg d$. Like the rippled-field magnetron discussed by Bekefi,[21] the beam circulates continuously through the wiggler field thereby providing a long effective interaction region. Unlike the rippled-field magnetron,[21] which operates at Brillouin flow, the present analysis assumes a tenuous electron beam with low density ($\omega_p^2 \ll \Omega_c^2$). In addition, it is assumed that the average transverse motion $V_y^0 = -cE_0/B_0$ is maintained by an applied electric field $E_0\hat{e}_x$ [Fig. 1(a)]. However, a completely analogous stability analysis can be developed for the case where the circulating electron motion corresponds to a large-orbit (cyclotron) gyration in the applied field $B_0\hat{e}_z$.

The present theoretical model (Sec. II) is based on the macroscopic, relativistic cold-fluid equations [Eqs. (5) and (6)] coupled with Maxwell's equations [Eqs. (8) and (9)], where it is assumed that the wave perturbations have ordinary-mode polarization with $\delta \mathbf{E} = \delta E_z \hat{e}_z$ and $\delta \mathbf{B} = \delta B_x \hat{e}_x + \delta B_y \hat{e}_y$. The electron beam density is assumed to be sufficiently low that equilibrium self-field effects are negligibly small and the Compton-regime approximation is valid with negligibly small perturbation in electrostatic potential ($\delta\phi \simeq 0$). In Sec. III, the equilibrium flow is examined in the limit of small wiggler amplitude $e^2 B_w^2/m^2c^4k_0^2 \ll 1$ [Eq. (25)] and weak spatial variation in electron energy $\gamma_0(x)mc^2$ across the anode–cathode gap [Eq. (26)]. The average equilibrium electron flow is then approximately $V_y^0 = V_E = -cE_0/B_0$ [Eq. (27)] with a small wiggler-induced modulation of the axial flow velocity $V_z^0 = -(eB_w/\hat{\gamma}mck_0)\cos k_0 y$. For ordinary-mode perturbations with $\partial/\partial z = 0$, detailed stability properties can be determined from the coupled eigenvalue

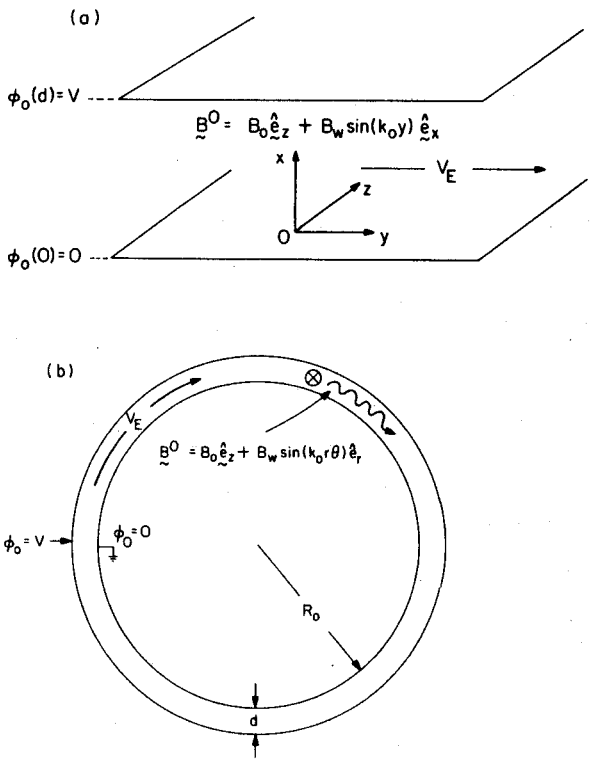

FIG. 1. Cross-field FEL configuration in (a) a planar geometry approximation, and (b) cylindrical geometry.

 0031-9171/84/010233-09$01.90

equations [(28)–(33)] or approximately from Eqs. (38)–(42) in the limit of weak transverse spatial variations with $|\partial/\partial x| \ll |\partial/\partial y|$. For small wiggler amplitude and beam density, the resulting matrix dispersion equation (47) can be approximated by the diagonal terms which give the dispersion relation [Eq. (50)]

$$\omega^2 - c^2k^2 - \omega_p^2 = -\omega_p^2\left(\frac{\Omega_w}{2ck_0}\right)^2\left(\frac{\omega}{[\omega-(k+k_0)V_E]} + \frac{\omega}{[\omega-(k-k_0)V_E]} + \frac{\omega(k+k_0)V_E - c^2(k+k_0)^2}{[\omega-(k+k_0)V_E]^2 - \Omega_c^2/\gamma_E^2} + \frac{\omega(k-k_0)V_E - c^2(k-k_0)^2}{[\omega-(k-k_0)V_E]^2 - \Omega_c^2/\gamma_E^2}\right),$$

where $\omega_p^2 = 4\pi n_b e^2/\gamma_E m$, $\Omega_w = eB_w/\gamma_E mc$, $\Omega_c = eB_0/\gamma_E mc$, $\gamma_E = (1 - V_E^2/c^2)^{-1/2}$, $\mathbf{k} = k\hat{\mathbf{e}}_y$ is the wave vector, and ω is the complex oscillation frequency.

Analytic and numerical estimates (Sec. IV) of the FEL growth rate obtained from Eq. (50) show that the upshifted resonance term proportional to $[\omega - (k + k_0)V_E]^{-1}$ in Eq. (50) leads to instability with characteristic maximum growth rate [Eq. (56)]

$$\mathrm{Im}(\delta\omega) = (\omega_p/2\sqrt{2})(\Omega_w/ck_0),$$

and emission frequency [Eq. (54)]

$$\omega_r = (1+\beta_E)\gamma_E^2 k_0 V_E,$$

where $\beta_E = V_E/c$. Depending on the size of Ω_w/ck_0, Eq. (56) can correspond to relatively short exponentiation times in units of ω_p^{-1}.

The resonance term proportional to $\{[\omega - (k + k_0)V_E]^2 - \Omega_c^2/\gamma_E^2\}^{-1}$ in Eq. (50) also leads to instability with characteristic maximum growth rate [Eq. (67)]

$$\mathrm{Im}(\delta\omega) = \frac{1}{4}\omega_p\left(\frac{\Omega_w}{ck_0}\right)\left(\frac{k_0c\gamma_E}{\Omega_c}\right)^{1/2}\left((1+\beta_E) - \frac{\Omega_c}{\gamma_E k_0 c}\right)^{1/2} \times \frac{(1-\Omega_c/\gamma_E k_0 c)^{1/2}}{(\beta_E - \Omega_c/\gamma_E k_0 c)^{1/2}},$$

and downshifted frequency [Eq. (62)]

$$\omega_r = (1+\beta_E)\gamma_E^2(\beta_E - \Omega_c/\gamma_E k_0 c)k_0 c.$$

Depending on the size of Ω_w/ck_0, Eq. (67) can give even shorter exponentiation times provided β_E is close to $\Omega_c/\gamma_E k_0 c$, although the output frequency is lower than that of Eq. (54).

The organization of this paper is the following. In Sec. II we outline the assumptions and macroscopic cold-fluid model used in the present analysis. The equilibrium flow and linearized Maxwell-fluid equations for ordinary-mode wave perturbations are discussed in Sec. III. Analytic and numerical studies of the resulting coupled eigenvalue equations (38)–(42) are presented in Sec. IV in the limit of weak transverse spatial variations [Eq. (35)] and low beam density ($\omega_p^2 \ll c^2k_0^2$) and wiggler amplitude ($\Omega_w^2 \ll c^2k_0^2$).

II. THEORETICAL MODEL AND ASSUMPTIONS

For present purposes, we consider the planar geometry illustrated in Fig. 1(a) with applied fields

$$\mathbf{E}^0 = E_0\hat{\mathbf{e}}_x, \qquad \mathbf{B}^0 = B_0\hat{\mathbf{e}}_z + \hat{\mathbf{e}}_x B_w \sin k_0 y, \tag{1}$$

where $B_0 = \text{const}$ is the axial magnetic field, $B_w = \text{const}$ is the transverse wiggler amplitude, $\lambda_0 = 2\pi/k_0 = \text{const}$ is the wiggler wavelength, $V = -E_0 d$ is the applied voltage, d is the anode–cathode spacing, and E_0 is the electric field. The planar configuration in Fig. 1(a) is used to model the cylindrical geometry in Fig. 1(b) in the limit of large aspect ratio $R_0 \gg d$. The assumption of constant wiggler amplitude $B_w = \text{const}$ is a valid approximation over the transverse extent of the electron beam provided $k_0 d \ll 1$, which we assume to be the case. In the present analysis, it is assumed that the electron beam is infinite in extent in the y and z directions with uniform average density n_b between $x = 0$ and $x = d$. It is also assumed that the beam density is sufficiently tenuous that the effects of equilibrium self-fields $\mathbf{E}_s^0$ and $\mathbf{B}_s^0$ can be neglected in comparison with the applied field components in Eq. (1). For example, it is readily shown from Poisson's equation that $|\mathbf{E}_s^0| \ll |E_0|$ provided

$$\tfrac{1}{2}(\omega_p^2 d^2/c^2) \ll eV/\hat{\gamma}mc^2, \tag{2}$$

where c is the speed of light *in vacuo*, $-e$ is the electron charge, m is the electron rest mass, $\omega_p^2 = 4\pi n_b e^2/\hat{\gamma}m$ is the relativistic plasma frequency squared, and $\hat{\gamma}mc^2$ is the characteristic electron energy. For the configuration illustrated in Fig. 1(a), the average equilibrium flow is primarily in the y direction at the $\mathbf{E}^0 \times \mathbf{B}^0$ velocity V_E, where

$$V_E = -cE_0/B_0 = cV/B_0 d. \tag{3}$$

In the present analysis, all equilibrium and perturbed quantities are allowed to have spatial variations only in the x and y directions with $\nabla = \hat{\mathbf{e}}_x(\partial/\partial x) + \hat{\mathbf{e}}_y(\partial/\partial y)$ and $\partial/\partial z = 0$. It is assumed that the beam density is sufficiently tenuous that the Compton-regime approximation is valid with negligibly small perturbations in electrostatic potential ($\delta\phi \simeq 0$). In particular, we consider perturbed electromagnetic fields $\delta\mathbf{E}$ and $\delta\mathbf{B}$ with ordinary-mode polarization

$$\delta\mathbf{E} = \delta E_z(x,y,t)\hat{\mathbf{e}}_z = -\frac{1}{c}\frac{\partial}{\partial t}\delta A_z(x,y,t)\hat{\mathbf{e}}_z,$$
$$\delta\mathbf{B} = \delta B_x(x,y,t)\hat{\mathbf{e}}_x + \delta B_y(x,y,t)\hat{\mathbf{e}}_y = \frac{\partial}{\partial y}\delta A_z(x,y,t)\hat{\mathbf{e}}_x - \frac{\partial}{\partial x}\delta A_z(x,y,t)\hat{\mathbf{e}}_y, \tag{4}$$

where $\delta\mathbf{B} = \nabla\times\delta\mathbf{A}$, $\delta\mathbf{E} = -(1/c)(\partial/\partial t)\delta\mathbf{A}$, and $\delta\mathbf{A}$

$= \delta A_z(x,y,t)\hat{e}_z$ is the perturbed vector potential. Finally, to complete the theoretical model, we make use of a macroscopic cold-fluid description in which the electron density $n(x,y,t)$ evolves according to the continuity equation

$$\left(\frac{\partial}{\partial t} + V_x \frac{\partial}{\partial x} + V_y \frac{\partial}{\partial y}\right) n = -n\left(\frac{\partial V_x}{\partial x} + \frac{\partial V_y}{\partial y}\right), \tag{5}$$

and the average electron flow velocity $\mathbf{V} = V_x(x,y,t)\hat{e}_x + V_y(x,y,t)\hat{e}_y + V_z(x,y,t)\hat{e}_z$ satisfies the relativistic cold-fluid momentum transfer equation

$$\left(\frac{\partial}{\partial t} + V_x \frac{\partial}{\partial x} + V_y \frac{\partial}{\partial y}\right)(\gamma m \mathbf{V})$$

$$= -e(\mathbf{E}^0 + \delta\mathbf{E}) - \frac{e}{c}\mathbf{V}\times(\mathbf{B}^0 + \delta\mathbf{B}). \tag{6}$$

Here, $\mathbf{E}^0 + \delta\mathbf{E}$ and $\mathbf{B}^0 + \delta\mathbf{B}$ are defined in Eqs. (1) and (4), and $\gamma(x,y,t)$ is the relativistic mass factor for a fluid element

$$\gamma = \left(1 - \frac{V_x^2}{c^2} - \frac{V_y^2}{c^2} - \frac{V_z^2}{c^2}\right)^{-1/2}. \tag{7}$$

Moreover, making use of Eq. (4), the $\nabla\times\delta\mathbf{B}$ Maxwell equation can be expressed as

$$\left(\frac{\partial^2}{\partial x^2} + \frac{\partial^2}{\partial y^2} - \frac{1}{c^2}\frac{\partial^2}{\partial t^2}\right)\delta A_z = -\frac{4\pi}{c}\delta J_z, \tag{8}$$

where the perturbed axial current $\delta J_z(x,y,t)$ is given by

$$\delta J_z = -en_0\delta V_z - eV_z^0\delta n. \tag{9}$$

Here, we have expressed quantities as an equilibrium value $(\partial/\partial t) = 0$ plus a perturbation, e.g., $n(x,y,t) = n_0(x,y) + \delta n(x,y,t)$, etc. As a further useful dynamical equation, we take the vector dot product of Eq. (6) with the flow velocity $\mathbf{V}$. This gives

$$\left(\frac{\partial}{\partial t} + V_x \frac{\partial}{\partial x} + V_y \frac{\partial}{\partial y}\right)\gamma mc^2 = -eE_0V_x + \frac{e}{c}V_z\frac{\partial}{\partial t}\delta A_z, \tag{10}$$

which describes the evolution of the energy γmc^2.

To summarize, Eqs. (5), (6), and (8), supplemented by the definitions in Eqs. (1), (4), and (7), constitute the final set of fluid-Maxwell equations used in the subsequent analysis. These equations describe the equilibrium $(\partial/\partial t = 0)$ and ordinary-mode stability properties of a tenuous electron beam propagating in the planar configuration illustrated in Fig. 1(a), assuming negligibly small beam thermal effects and equilibrium self-fields. For future reference, an important simplification occurs in the exact dynamical equation (6). We introduce the vector potential $A_{wz}(y)$ for the wiggler field in Eq. (1) such that $B_w \sin k_0 y = (\partial/\partial y)A_{wz}(y)$, where

$$A_{wz}(y) = -(B_w/k_0)\cos k_0 y. \tag{11}$$

After some straightforward algebraic manipulation, the z component of Eq. (6) can be expressed (exactly) in the equivalent form

$$\left(\frac{\partial}{\partial t} + V_x \frac{\partial}{\partial x} + V_y \frac{\partial}{\partial y}\right)\left(\gamma mV_z - \frac{e}{c}A_{wz} - \frac{e}{c}\delta A_z\right) = 0, \tag{12}$$

corresponding to the conservation of axial canonical momentum $P_z = \gamma mV_z - (e/c)A_{wz} - (e/c)\delta A_z = \text{const}$ following a fluid element. If we consider the case where there is no axial flow in the absence of wiggler and radiation fields, then $P_z = 0$ and Eq. (12) gives the exact result

$$\gamma mV_z = (e/c)A_{wz} + (e/c)\delta A_z. \tag{13}$$

Making use of Eq. (13) to eliminate V_z from the x and y components of motion in Eq. (6) then gives

$$\left(\frac{\partial}{\partial t} + V_x \frac{\partial}{\partial x} + V_y \frac{\partial}{\partial y}\right)(\gamma mV_x)$$

$$= -eE_0 - \frac{eB_0}{c}V_y - \frac{e^2}{2\gamma mc^2}\frac{\partial}{\partial x}(A_{wz} + \delta A_z)^2, \tag{14}$$

$$\left(\frac{\partial}{\partial t} + V_x \frac{\partial}{\partial x} + V_y \frac{\partial}{\partial y}\right)(\gamma mV_y)$$

$$= \frac{eB_0}{c}V_x - \frac{e^2}{2\gamma mc^2}\frac{\partial}{\partial y}(A_{wz} + \delta A_z)^2. \tag{15}$$

With regard to the transverse motion of an electron fluid element, it is evident directly from Eqs. (14) and (15) that $(A_{wz} + \delta A_z)^2$ plays the role of a ponderomotive potential for the combined wiggler and radiation fields.

III. GENERAL EQUILIBRIUM AND LINEARIZED STABILITY EQUATIONS

In this section, we make use of the theoretical model outlined in Sec. II to investigate equilibrium and stability properties for the planar flow configuration illustrated in Fig. 1(a).

A. Equilibrium equations

From Eqs. (13)–(15), the exact equilibrium $(\partial/\partial t = 0)$ motion of a fluid element in the absence of radiation field $(\delta A_z = 0)$ is determined from

$$V_z^0 = \frac{e}{\gamma_0 mc}A_{wz} = -\frac{eB_w}{\gamma_0 mck_0}\cos k_0 y, \tag{16}$$

$$\left(V_x^0\frac{\partial}{\partial x} + V_y^0\frac{\partial}{\partial y}\right)(\gamma_0 mV_x^0) = -eE_0 - \frac{eB_0}{c}V_y^0, \tag{17}$$

$$\left(V_x^0\frac{\partial}{\partial x} + V_y^0\frac{\partial}{\partial y}\right)(\gamma_0 mV_y^0)$$

$$= \frac{eB_0}{c}V_x^0 - \frac{e^2}{2\gamma_0 mc^2}\frac{\partial}{\partial y}(A_{wz})^2, \tag{18}$$

where

$$\gamma_0 = \left(1 - \frac{V_x^{02}}{c^2} - \frac{V_y^{02}}{c^2} - \frac{V_z^{02}}{c^2}\right)^{-1/2}, \tag{19}$$

and

$$\left(V_x^0\frac{\partial}{\partial x} + V_y^0\frac{\partial}{\partial y}\right)(\gamma_0 mc^2 + eE_0x) = 0, \tag{20}$$

follows from Eq. (10). Making use of Eq. (5), the equilibrium density profile $n_0(x,y)$ is related self-consistently to the flow velocity by

$$\left(V_x^0\frac{\partial}{\partial x} + V_y^0\frac{\partial}{\partial y}\right)n_0 = -n_0\left(\frac{\partial}{\partial x}V_x^0 + \frac{\partial}{\partial y}V_y^0\right). \tag{21}$$

Integrating Eq. (20), and defining $\hat{\gamma} \equiv \gamma_0(x=0)$, gives

$$\gamma_0 = \hat{\gamma}(1 + eVx/\hat{\gamma}mc^2 d), \tag{22}$$

where $V = -E_0 d$ is the applied voltage. Moreover, making use of Eq. (16) to eliminate V_z^0 from the definition of γ_0, we find from Eqs. (19) and (22) that

$$\frac{V_x^{02}}{c^2} + \frac{V_y^{02}}{c^2} = 1 - \left(1 + \frac{e^2 B_w^2}{m^2 c^2 k_0^2}\cos^2 k_0 y\right)\frac{1}{\hat{\gamma}^2}\left(1 + \frac{eVx}{\gamma mc^2 d}\right)^{-2}. \tag{23}$$

Although closed expressions for the individual velocity components V_x^0 and V_y^0 are difficult to obtain analytically from Eqs. (17) and (18), the combination $V_x^{02} + V_y^{02}$ is determined exactly by Eq. (23) in the present model.

For future reference, we summarize equilibrium flow properties in circumstances where the x-z motion is nonrelativistic with

$$\gamma_0^2(V_x^{02}/c^2), \quad \gamma_0^2(V_z^{02}/c^2) \ll 1, \tag{24}$$

but the y motion is generally relativistic with V_y^0 approximately equal to the $\mathbf{E}^0 \times \mathbf{B}^0$ velocity $V_E = -cE_0/B_0$. From Eq. (16), the inequality $\gamma_0^2 V_z^{02}/c^2 \ll 1$ implies weak wiggler amplitude with

$$e^2 B_w^2/m^2 c^4 k_0^2 \ll 1. \tag{25}$$

If, in addition, it is assumed that the spatial variation in γ_0 is weak over the gap region $0 \leqslant x \leqslant d$, then $eV/\hat{\gamma}mc^2 \ll 1$, or equivalently,

$$(V_E/c)(\Omega_c d/c) \ll 1, \tag{26}$$

where $V_E = -cE_0/B_0 = cV/B_0 d$ and $\Omega_c = eB_0/\hat{\gamma}mc$. Even if $V_E \simeq c$, Eq. (26) is satisfied provided $0.6\, B_0 d \ll \hat{\gamma}$, where B_0 is in kilogauss and d is in centimeters. On the other hand, Eq. (25) is satisfied provided $0.6\, B_w k_0^{-1} \ll 1$, where B_w is in kilogauss and k_0^{-1} is in centimeters. Making use of Eqs. (24)–(26), it is straightforward to show from Eqs. (10)–(18) and (22) that the equilibrium flow correct to $O(B_w)$ is given by

$$\begin{aligned} V_z^0 &= (eB_w/\hat{\gamma}mck_0)\cos k_0 y, \\ V_y^0 &= V_E + O(B_w^2), \\ V_x^0 &= O(B_w^2), \end{aligned} \tag{27}$$

where $\hat{\gamma} \simeq (1 - V_E^2/c^2)^{-1/2}$ and $\gamma_0 \simeq \hat{\gamma}$ is approximately uniform over the region $0 \leqslant x \leqslant d$. For small wiggler amplitude [Eq. (25)], the wiggler field produces only a small second-order modulation of the x-y motion [Eqs. (23) and (27)], with V_x^0 and V_y^0 given approximately by $V_x^0 = 0$ and $V_y^0 = V_E$. Finally, in the context of Eqs. (21) and (27), a uniform density profile with $n_0(x,y) = n_b = \text{const}$ is an allowed equilibrium solution in the region $0 \leqslant x \leqslant d$ [Fig. 1(a)].

B. Linearized Maxwell-fluid equations

We now examine stability properties for small-amplitude perturbations about the exact equilibrium flow equations (16)–(21). All perturbation quantities $\delta\psi(x,y,t)$ are expressed as

$$\delta\psi(x,y,t) = \delta\hat{\psi}(x,y)\exp(-i\omega t),$$

where $\mathrm{Im}\,\omega > 0$ for the case of oscillations that amplify temporally. Making use of Eqs. (16)–(21), we find from Eqs. (13)–(15) that

$$\delta\hat{V}_z = \frac{\delta\hat{\gamma}}{\gamma_0}\frac{eB_w}{\gamma_0 mck_0}\cos k_0 y + \frac{e\delta\hat{A}_z}{\gamma_0 mc}, \tag{28}$$

$$\left(-i\omega + V_x^0\frac{\partial}{\partial x} + V_y^0\frac{\partial}{\partial y}\right)(\gamma_0 m\delta\hat{V}_x + \delta\hat{\gamma}mV_x^0) + \left(\delta\hat{V}_x\frac{\partial}{\partial x} + \delta\hat{V}_y\frac{\partial}{\partial y}\right)(\gamma_0 mV_x^0) = -\frac{eB_0}{c}\delta\hat{V}_y + \frac{e^2 B_w}{\gamma_0 mc^2 k_0}\cos k_0 y\frac{\partial}{\partial x}\delta\hat{A}_z, \tag{29}$$

$$\left(-i\omega + V_x^0\frac{\partial}{\partial x} + V_y^0\frac{\partial}{\partial y}\right)(\gamma_0 m\delta\hat{V}_y + \delta\hat{\gamma}mV_y^0) + \left(\delta\hat{V}_x\frac{\partial}{\partial x} + \delta\hat{V}_y\frac{\partial}{\partial y}\right)(\gamma_0 mV_y^0) = \frac{eB_0}{c}\delta\hat{V}_x + \frac{e^2 B_w}{\gamma_0 mc^2 k_0}\frac{\partial}{\partial y}(\cos k_0 y\delta\hat{A}_z), \tag{30}$$

where use has been made of $A_{wz} = -(B_w/k_0)\cos k_0 y$ and $V_z^0 = -(eB_w/\gamma_0 mck_0)\cos k_0 y$. Making use of $\delta V_x(\partial/\partial x)\gamma_0 mc^2 = -eE_0\delta V_x$ [Eq. (22)], the linearized energy equation (10) can be expressed as

$$\left(-i\omega + V_x^0\frac{\partial}{\partial x} + V_y^0\frac{\partial}{\partial y}\right)\delta\hat{\gamma} = i\omega\frac{e^2 B_w}{\gamma_0 mc^2}\cos k_0 y\delta\hat{A}_z. \tag{31}$$

Equations (28)–(31) determine the perturbed fluid motion $(\delta\hat{V}_x, \delta\hat{V}_y, \delta\hat{V}_z, \delta\hat{\gamma})$ in terms of the wiggler field and $\delta\hat{A}_z$. Returning to the Maxwell equation (8) for δA_z, we make use of Eq. (28) to eliminate δV_z. Equation (8) then reduces to

$$\left(\frac{\partial^2}{\partial x^2} + \frac{\partial^2}{\partial y^2} + \frac{\omega^2}{c^2} - \frac{4\pi n_0 e^2}{\gamma_0 mc^2}\right)\delta\hat{A}_z = \frac{4\pi n_0 e^2}{\gamma_0 mc^2}\frac{B_w}{k_0}\cos k_0 y\left(\frac{\delta\hat{\gamma}}{\gamma_0} - \frac{\delta\hat{n}}{n_0}\right). \tag{32}$$

In Eq. (32), $\delta\hat{\gamma}(x,y)$ is related to $\delta\hat{A}_z(x,y)$ by Eq. (31), and $\delta\hat{n}(x,y)$ is determined in terms of the perturbed flow from the linearized continuity equation (5), i.e.,

$$\left(-i\omega + V_x^0\frac{\partial}{\partial x} + V_y^0\frac{\partial}{\partial y}\right)\delta\hat{n} + \delta\hat{n}\left(\frac{\partial V_x^0}{\partial x} + \frac{\partial V_y^0}{\partial y}\right) = -\left(\delta\hat{V}_x\frac{\partial n_0}{\partial x} + \delta\hat{V}_y\frac{\partial n_0}{\partial y}\right) - n_0\left(\frac{\partial}{\partial x}\delta\hat{V}_x + \frac{\partial}{\partial y}\delta\hat{V}_y\right). \tag{33}$$

To summarize, Eqs. (29)–(33) constitute the final coupled eigenvalue equations for $\delta\hat{A}_z(x,y)$, $\delta\hat{n}(x,y)$, $\delta\hat{\gamma}(x,y)$, $\delta\hat{V}_x(x,y)$, and $\delta\hat{V}_y(x,y)$ assuming ordinary-mode perturbations about the general equilibrium flow equations (16)–(21). Equations (29)–(33) include both x and y variations and must be solved numerically in the general case. In the special limit of zero wiggler amplitude ($B_w = 0$), it follows trivially that

$\delta\hat{V}_x = 0, \delta\hat{V}_y = 0, \delta\hat{\gamma} = 0$, and $\delta\hat{n} = 0$, and Eq. (32) reduces to the familiar ordinary-mode eigenvalue equation

$$\left(\frac{\partial^2}{\partial x^2} + \frac{\partial^2}{\partial y^2} + \frac{\omega^2}{c^2} - \frac{4\pi n_0 e^2}{\gamma_0 mc^2}\right)\delta\hat{A}_z = 0, \tag{34}$$

for a cold plasma in the absence of wiggler field.

IV. ANALYSIS OF EIGENVALUE EQUATION

In general, allowing for full x and y dependence, the coupled eigenvalue equations (29)–(33) must be solved numerically. In this regard, Eqs. (29)–(33) can be used to investigate cross-field free electron laser stability properties over a broad parameter range where the tenuous-beam theory summarized in Secs. II and III is valid. For present purposes, however, to illustrate the basic physics features of the cross-field FEL instability, we consider the regime where spatial variations in the y direction have short wavelength in comparison with spatial variations in the x direction, i.e.,

$$\left|\frac{\partial}{\partial y}\right| > \left|\frac{\partial}{\partial x}\right|. \tag{35}$$

In particular, we neglect the x dependence of all equilibrium and perturbation quantities in Eqs. (29)–(33) ($\partial/\partial x = 0$). In addition, it is assumed that the inequalities in Eqs. (24)–(26) are satisfied, and the equilibrium x-y motion is approximated by

$$V_x^0 = 0, \qquad V_y^0 = V_E = -cE_0/B_0. \tag{36}$$

It is convenient to define

$$\Omega_c = eB_0/\gamma_E mc, \quad \Omega_w = eB_w/\gamma_E mc, \qquad \omega_p^2 = 4\pi n_b e^2/\gamma_E m, \quad \delta\tilde{A}_z = e\delta\hat{A}_z/\gamma_E mc^2, \tag{37}$$

where $\gamma_E = (1 - V_E^2/c^2)^{-1/2} = \text{const}$, and $n_b = \text{const}$ is the (uniform) beam density. Setting $\partial/\partial x = 0$ and making use of Eq. (36), the coupled eigenvalue equations (29)–(33) can be approximated by

$$\left(-i\omega + V_E\frac{\partial}{\partial y}\right)\delta\hat{V}_x = -\Omega_c\delta\hat{V}_y, \tag{38}$$

$$\left(-i\omega + V_E\frac{\partial}{\partial y}\right)\delta\hat{V}_y + V_E\left(-i\omega + V_E\frac{\partial}{\partial y}\right)\frac{\delta\hat{\gamma}}{\gamma_E} + \Omega_c\frac{V_E^2}{c^2}\delta\hat{V}_x = \Omega_c\delta\hat{V}_x + \frac{\Omega_w}{ck_0}c^2\frac{\partial}{\partial y}(\cos k_0 y\delta\tilde{A}_z), \tag{39}$$

$$\left(-i\omega + V_E\frac{\partial}{\partial y}\right)\frac{\delta\hat{\gamma}}{\gamma_E} = i\omega\frac{\Omega_w}{ck_0}\cos k_0 y\delta\tilde{A}_z, \tag{40}$$

$$\left(\frac{\partial^2}{\partial y^2} + \frac{\omega^2}{c^2} - \frac{\omega_p^2}{c^2}\right)\delta\tilde{A}_z = -\frac{\omega_p^2}{c^2}\frac{\Omega_w}{ck_0}\cos k_0 y\left(\frac{\delta\hat{n}}{n_b} - \frac{\delta\hat{\gamma}}{\gamma_E}\right), \tag{41}$$

$$\left(-i\omega + V_E\frac{\partial}{\partial y}\right)\delta\hat{n} = -n_b\frac{\partial}{\partial y}\delta\hat{V}_y. \tag{42}$$

Equations (38)–(42) constitute coupled equations for $\delta\hat{V}_x(y)$, $\delta\hat{V}_y(y)$, $\delta\hat{\gamma}(y)$, $\delta\tilde{A}_z(y)$, and $\delta\hat{n}(y)$. In obtaining the term $\Omega_c(V_E^2/c^2)\delta\hat{V}_x$ in Eq. (39), we have made use of Eq. (22) to approximate $\delta\hat{V}_x(\partial/\partial x)(\gamma_0 mV_y^0) = (V_E/c^2)\delta\hat{V}_x(-eE_0) = \Omega_c(V_E^2/c^2)\delta\hat{V}_x$ in Eq. (30).

We now Fourier decompose with respect to the y dependence in Eqs. (38)–(42) with $\delta\hat{A}_z(y) = \Sigma_k\delta\hat{A}_k\exp(iky)$, etc. After some straightforward algebra, this gives

$$\delta\hat{\gamma}_k = -\gamma_E[\omega/(\omega - kV_E)](\Omega_w/2ck_0)\times(\delta\tilde{A}_{k+k_0} + \delta\tilde{A}_{k-k_0}), \tag{43}$$

$$\delta\hat{n}_k = n_b k\delta\hat{V}_{y,k}/(\omega - kV_E), \tag{44}$$

$$\delta\hat{V}_{y,k} = \frac{\Omega_w}{2ck_0}\frac{(\omega - kV_E)(\omega V_E - c^2k)}{[(\omega - kV_E)^2 - \Omega_c^2/\gamma_E^2]}\times(\delta\tilde{A}_{k+k_0} + \delta\tilde{A}_{k-k_0}), \tag{45}$$

$$(\omega^2 - c^2k^2 - \omega_p^2)\delta\tilde{A}_k = -\omega_p^2\frac{\Omega_w}{2ck_0}\left(\frac{1}{n_b}(\delta\hat{n}_{k+k_0} + \delta\hat{n}_{k-k_0}) - \frac{1}{\gamma_E}(\delta\hat{\gamma}_{k+k_0} + \delta\hat{\gamma}_{k-k_0})\right). \tag{46}$$

Combining Eqs. (43)–(45) and substituting into Eq. (46) gives the final eigenvalue equation

$$\left(1 - \frac{c^2k^2}{\omega^2} - \frac{\omega_p^2}{\omega^2} + \chi_{k+k_0}(\omega) + \chi_{k-k_0}(\omega)\right)\delta\tilde{A}_k + \chi_{k+k_0}(\omega)\delta\tilde{A}_{k+2k_0} + \chi_{k-k_0}(\omega)\delta\tilde{A}_{k-2k_0} = 0, \tag{47}$$

where the wiggler-induced susceptibility $\chi_k(\omega)$ is defined by

$$\chi_k(\omega) = \frac{\omega_p^2}{\omega^2}\left(\frac{\Omega_w}{2ck_0}\right)^2\times\left(\frac{(\omega kV_E - c^2k^2)}{[(\omega - kV_E)^2 - \Omega_c^2/\gamma_E^2]} + \frac{\omega}{(\omega - kV_E)}\right). \tag{48}$$

Equation (47) constitutes the final matrix dispersion equation for the cross-field free electron laser instability in circumstances where $\partial/\partial x = 0$ is assumed. For $\Omega_w^2/c^2k_0^2 \ll 1$ [Eq. (25)], the coupling to the off-diagonal terms in Eq. (47) is weak, and the dispersion relation can be approximated by

$$1 - c^2k^2/\omega^2 - \omega_p^2/\omega^2 = -[\chi_{k+k_0}(\omega) + \chi_{k-k_0}(\omega)], \tag{49}$$

or equivalently

$$\omega^2 - c^2k^2 - \omega_p^2 = -\omega_p^2\left(\frac{\Omega_w}{2ck_0}\right)^2\left(\frac{\omega}{[\omega - (k+k_0)V_E]} + \frac{\omega}{[\omega - (k-k_0)V_E]} + \frac{[\omega(k+k_0)V_E - c^2(k+k_0)^2]}{[\omega - (k+k_0)V_E]^2 - \Omega_c^2/\gamma_E^2} + \frac{[\omega(k-k_0)V_E - c^2(k-k_0)^2]}{[\omega - (k-k_0)V_E]^2 - \Omega_c^2/\gamma_E^2}\right). \tag{50}$$

Equation (50) constitutes the final ordinary-mode dis-

persion relation (diagonal approximation) in circumstances where $|k| \gg |\partial/\partial x|$ and spatial variations in the x direction are neglected. Equation (50) can be used to investigate cross-field free electron laser stability properties over a broad parameter range consistent with the Compton-regime approximation (tenuous beam and $\delta\phi \simeq 0$). In the remainder of this paper, we make use of Eq. (50) to obtain simple analytic estimates of stability properties (Sec. IV A) as well as detailed numerical calculations of free electron laser growth rates (Sec. IV B).

A. Analytic estimates of FEL growth rates

In this section, we make use of Eq. (50) to obtain simple analytic estimates of instability growth rates in the limit of small wiggler amplitude and beam density with

$$\Omega_w^2/4c^2k_0^2, \quad \omega_p^2/c^2k_0^2 \ll 1. \tag{51}$$

It is evident that the ordinary-mode electromagnetic wave with $\omega^2 - c^2k^2 - \omega_p^2 \simeq 0$ can resonantly couple to wiggler-induced current perturbations whenever the beam resonance condition $\omega - (k \pm k_0)V_E = 0$ or cyclotron resonance condition $[\omega - (k \pm k_0)V_E]^2 - \Omega_c^2/\gamma_E^2 = 0$ are approximately satisfied. Now we simplify Eq. (50) in these two limiting regimes.

1. FEL instability near beam resonance

Restricting attention to upshifted frequencies, we first examine Eq. (50) for (ω,k) in the vicinity of (ω_r,k_r) determined from

$$\begin{aligned} \omega_r &= (k_r^2c^2 + \omega_p^2)^{1/2}, \\ \omega_r &= (k_r + k_0)V_E, \end{aligned} \tag{52}$$

where $\omega_r > 0$ and $k_r > 0$ are assumed. In this case, Eq. (50) can be approximated by

$$[\omega - (k + k_0)V_E](\omega^2 - c^2k^2 - \omega_p^2) = -\omega_p^2(\Omega_w/2ck_0)^2\omega. \tag{53}$$

For $\omega_p^2/c^2k_0^2 \ll 1$, it follows from Eq. (52) that ω_r and k_r can be approximated by the familiar result

$$\begin{aligned} \omega_r &= (1 + \beta_E)\gamma_E^2k_0V_E, \\ k_r &= (1 + \beta_E)\gamma_E^2\beta_Ek_0, \end{aligned} \tag{54}$$

where $\gamma_E = (1 - \beta_E^2)^{-1/2}$. Expressing $\omega = \omega_r + \delta\omega$ and $k = k_r + \delta k$, and retaining terms to order $(\delta\omega)^2$ and $(\delta k)^2$, the dispersion relation (53) can be approximated by

$$\left(\delta\omega - \frac{c^2k_r}{\omega_r}\delta k\right)(\delta\omega - V_E\delta k) = -\frac{1}{2}\omega_p^2\left(\frac{\Omega_w}{2ck_0}\right)^2. \tag{55}$$

For $\delta k = 0$, Eq. (55) gives the characteristic maximum growth rate

$$\mathrm{Im}(\delta\omega) = (\omega_p/\sqrt{2})(\Omega_w/2ck_0). \tag{56}$$

Depending on the size of $(\Omega_w/2ck_0)$, Eq. (56) can correspond to relatively short exponentiation times in units of ω_p^{-1}. Within the range of validity of Eq. (55), it is readily shown that the growth rate is stabilized ($\mathrm{Im}\,\delta\omega = 0$) whenever $(\delta k)^2 \geqslant (\delta k)_M^2$, where

$$(\delta k)_M^2 = 2\frac{\omega_p^2}{V_E^2}\frac{k_r^2}{k_0^2}\left(\frac{\Omega_w}{2ck_0}\right)^2, \tag{57}$$

and k_r is defined in Eq. (54). Making use of Eq. (56) and substituting in Eq. (50), it is readily shown for $\omega \simeq (k + k_0) \times V_E$ that the cyclotron resonance term proportional to $\{[\omega - (k + k_0)V_E]^2 - \Omega_c^2/\gamma_E^2\}^{-1}$ is negligibly small provided

$$\frac{\omega_p}{\Omega_c}\frac{B_w}{B_0}\frac{\gamma_E^2(1 + \beta_E)}{\beta_E} \ll 2\sqrt{2}.$$

It is interesting to compare Eq. (53) with the cold-beam Compton-regime dispersion relation obtained in the case of zero guide field ($B_0 = 0$). Setting $\Omega_c = 0$ in Eq. (50) and denoting V_E by V_b, the quadratic resonance term $[\omega - (k + k_0)V_b]^{-2}$ dominates the linear resonance term $[\omega - (k + k_0)V_b]^{-1}$ on the right-hand side of Eq. (50), which leads to the approximate dispersion relation

$$\begin{aligned} &[\omega - (k + k_0)V_b]^2(\omega^2 - c^2k^2 - \omega_p^2) \\ &\quad = -\omega_p^2(\Omega_w/2ck_0)^2(k + k_0)[\omega V_b - c^2(k + k_0)], \end{aligned} \tag{58}$$

with characteristic maximum growth rate (for $\delta k = 0$)

$$\mathrm{Im}(\delta\omega) = \frac{\sqrt{3}}{2}\left(\frac{\omega_p^2}{c^2k_0^2}\frac{\Omega_w^2}{4c^2k_0^2}\right)^{1/3}\left(\frac{1 + \beta_b}{2\beta_b}\right)^{1/3}k_0c. \tag{59}$$

Typically, Eq. (59) gives a somewhat larger growth rate than Eq. (56).

2. FEL instability near cyclotron resonance

We now return to Eq. (50) in the presence of a guide field ($B_0 \neq 0$) and examine the dispersion relation for (ω,k) in the vicinity of (ω_r,k_r) corresponding to cyclotron resonance, i.e.,

$$\begin{aligned} \omega_r &= (k_r^2c^2 + \omega_p^2)^{1/2}, \\ \omega_r &= (k_r + k_0)V_E \pm \Omega_c/\gamma_E, \end{aligned} \tag{60}$$

where $\omega_r > 0$ and $k_r > 0$ are assumed. In this case, Eq. (50) can be approximated by

$$\begin{aligned} &\{[\omega - (k + k_0)V_E]^2 - \Omega_c^2/\gamma_E^2\}(\omega^2 - c^2k^2 - \omega_p^2) \\ &\quad = -\omega_p^2(\Omega_w/2ck_0)^2(k + k_0)[\omega V_E - c^2(k + k_0)]. \end{aligned} \tag{61}$$

For $\omega_p^2/c^2k_0^2 \ll 1$, it follows from Eq. (60) that ω_r and k_r can be approximated by

$$\begin{aligned} \omega_r &= (1 + \beta_E)\gamma_E^2(\beta_E \pm \Omega_c/\gamma_Ek_0c)k_0c, \\ k_r &= (1 + \beta_E)\gamma_E^2(\beta_E \pm \Omega_c/\gamma_Ek_0c)k_0. \end{aligned} \tag{62}$$

As before, we express $\omega = \omega_r + \delta\omega$ and $k = k_r + \delta k$ in Eq. (61). For $\delta k = 0$, some straightforward algebra shows that Eq. (61) can be approximated by

$$\begin{aligned} (\delta\omega)^3 \pm 2\left(\frac{\Omega_c}{\gamma_E}\right)(\delta\omega)^2 = \frac{\omega_p^2}{2}\left(\frac{\Omega_w}{2ck_0}\right)^2\left(\frac{k_r + k_0}{k_r}\right) \\ \times\left((1 + \beta_E)k_0c \pm \frac{\Omega_c}{\gamma_E}\right). \end{aligned} \tag{63}$$

For a sufficiently weak applied field B_0 such that $\Omega_c/\gamma_E k_0 c \ll 1$ and $\Omega_c/\gamma_E \ll |\delta\omega|$, Eq. (63) reduces to the unmagnetized results in Eqs. (58) and (59). On the other hand, for $\Omega_c/\gamma_E \gg |\delta\omega|$ the quadratic term in Eq. (63) dominates and $\delta\omega$ is determined from

$$(\delta\omega)^2 = \frac{\omega_p^2}{4}\left(\frac{\Omega_w}{2ck_0}\right)^2\left(\frac{k_r + k_0}{k_r}\right) \times\left(1 \pm (1+\beta_E)\frac{k_0 c\gamma_E}{\Omega_c}\right), \tag{64}$$

for $\delta k = 0$. Making use of Eq. (62) to eliminate k_r, Eq. (64) can be expressed in the equivalent form

$$(\delta\omega)^2 = \pm\frac{\omega_p^2}{4}\left(\frac{\Omega_w}{2ck_0}\right)^2\left(\frac{k_0 c\gamma_E}{\Omega_c}\right)\left((1+\beta_E) \pm \frac{\Omega_c}{\gamma_E k_0 c}\right) \times\frac{(1 \pm \Omega_c/\gamma_E k_0 c)}{(\beta_E \pm \Omega_c/\gamma_E k_0 c)}. \tag{65}$$

Clearly the + branch in Eq. (65) is always stable (Im $\delta\omega = 0$), whereas the − branch exhibits instability whenever

$$\Omega_c/\gamma_E k_0 c < \beta_E, \tag{66}$$

with corresponding growth rate

$$\mathrm{Im}(\delta\omega) = \frac{1}{4}\omega_p\left(\frac{\Omega_w}{ck_0}\right)\left(\frac{k_0 c\gamma_E}{\Omega_c}\right)^{1/2}\left((1+\beta_E) - \frac{\Omega_c}{\gamma_E k_0 c}\right)^{1/2} \times\frac{(1 - \Omega_c/\gamma_E k_0 c)^{1/2}}{(\beta_E - \Omega_c/\gamma_E k_0 c)^{1/2}}, \tag{67}$$

and downshifted emission frequency [Eq. (62)] $\omega_r = (1+\beta_E)\gamma_E^2(\beta_E - \Omega_c/\gamma_E k_0 c)k_0 c$. Making use of Eq. (67) and substituting in Eq. (50), it is readily shown for $\omega - (k + k_0)V_E \simeq -\Omega_c/\gamma_E$ that the linear resonance term proportional to $[\omega - (k + k_0)V_E]^{-1}$ is negligibly small provided

$$\frac{\omega_p}{2k_0 c}\frac{\Omega_w}{k_0 c}\left(\beta_E - \frac{\Omega_c}{k_0 c\gamma_E}\right)^{1/2} \ll\left(\frac{\Omega_c}{k_0 c\gamma_E}\right)^{1/2}\left(1 - \frac{\Omega_c}{k_0 c\gamma_E}\right)\left((1+\beta_E) - \frac{\Omega_c}{k_0 c\gamma_E}\right)^{1/2}.$$

B. Numerical results

The complete dispersion relation in Eq. (50) is an eighth-order algebraic equation for the complex oscillation frequency ω. In this regard, Eq. (50) has been solved numerically and typical results are summarized in Figs. 2 and 3, where the normalized growth rate (Im ω)/ck_0 is plotted versus k/k_0 for the unstable branch with upshifted wavenumber $k \sim k_r = (1+\beta_E)\gamma_E^2\beta_E k_0$. In Fig. 2, we fix $\gamma_E = 2$, $\Omega_c/ck_0 = 0.5$, and $\omega_p^2/c^2k_0^2 = 0.1$ and vary B_w/B_0 from 0.1 [Fig. 2(a)] to 0.5 [Fig. 2(c)]. On the other hand, in Fig. 3, we fix $\gamma_E = 2$, $\Omega_c/ck_0 = 0.5$, and $B_w/B_0 = 0.25$ and vary $\omega_p^2/c^2k_0^2$ from 0.25 [Fig. 3(a)] to 0.5 [Fig. 3(b)]. For small values of both B_w/B_0 and $\omega_p^2/c^2k_0^2$, it is clear from Fig. 2(a) that the bandwidth of unstable k values is very narrow. Indeed, $\Delta k/k_r \sim 10^{-2}$ for the parameters in Fig. 2(a). However, for increasing values of B_w/B_0 (Fig. 2), or for increasing values of

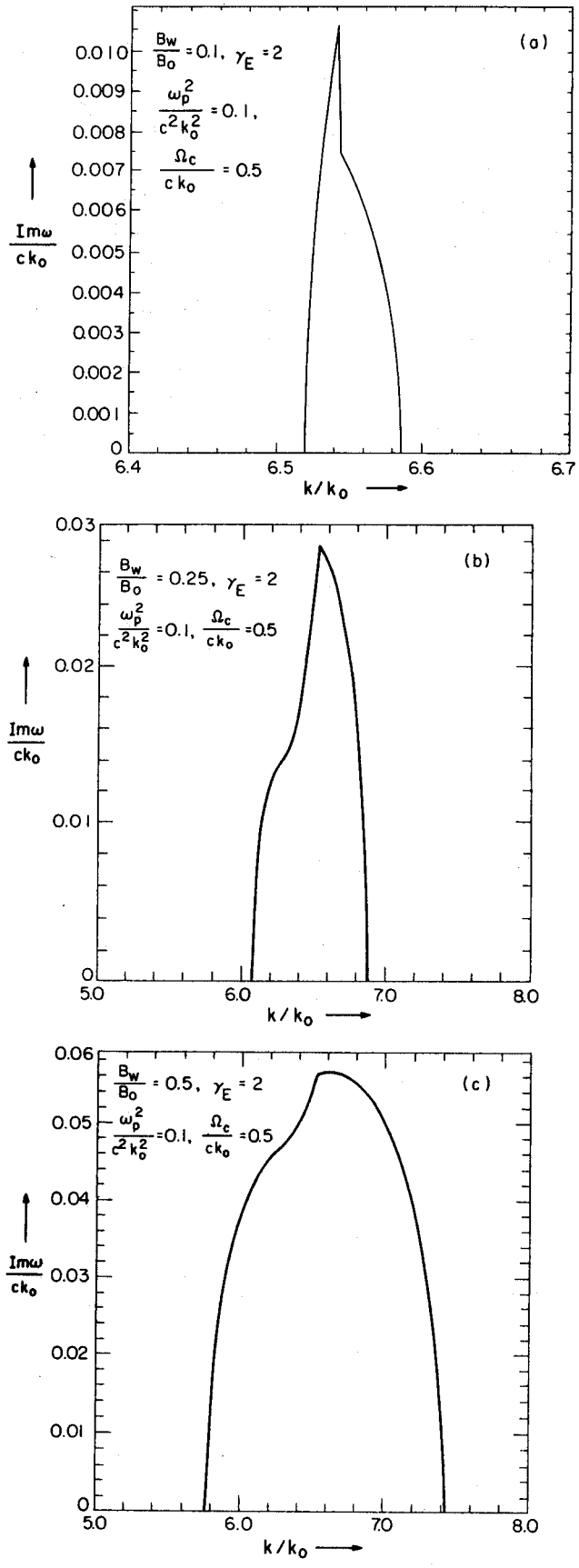

FIG. 2. Plot of the normalized growth rate Im ω/ck_0 vs k/k_0 obtained numerically from Eq. (50) for the upshifted unstable mode with $\omega \simeq (k + k_0)V_E$. Parameters correspond to $\gamma_E = 2$, $\omega_p^2/c^2k_0^2 = 0.1$, $\Omega_c/ck_0 = 0.5$, and (a) $B_w/B_0 = 0.1$, (b) $B_w/B_0 = 0.25$, and (c) $B_w/B_0 = 0.5$.

$\omega_p^2/c^2k_0^2$ (Fig. 3), both the bandwidth of unstable k values and the maximum growth rate $(\mathrm{Im}\,\omega)_{MAX}$ increase substantially. The "dimpled" structure of the $\mathrm{Im}\,\omega/ck_0$ vs k/k_0 plots in Figs. 2 and 3 has to do with the high-order (eighth-order) nature of the algebraic dispersion relation for ω in Eq. (50).

Finally, we have also solved numerically the complete dispersion relation (50) for the unstable downshifted branch near cyclotron resonance with $\omega - (k + k_0)V_E \simeq -\Omega_c/\gamma_E$. (See discussion at the end of Sec. IV A.) Typical numerical results are illustrated in Fig. 4 for parameters such that the growth rate of the downshifted branch is comparable to the cross-field FEL growth rates in Figs. 2 and 3. Note from Fig. 4 than an increase in B_w/B_0 or $\omega_p^2/c^2k_0^2$ leads to an increase in growth rate $\mathrm{Im}\,\omega$ and a broadening of the range of unstable k values.

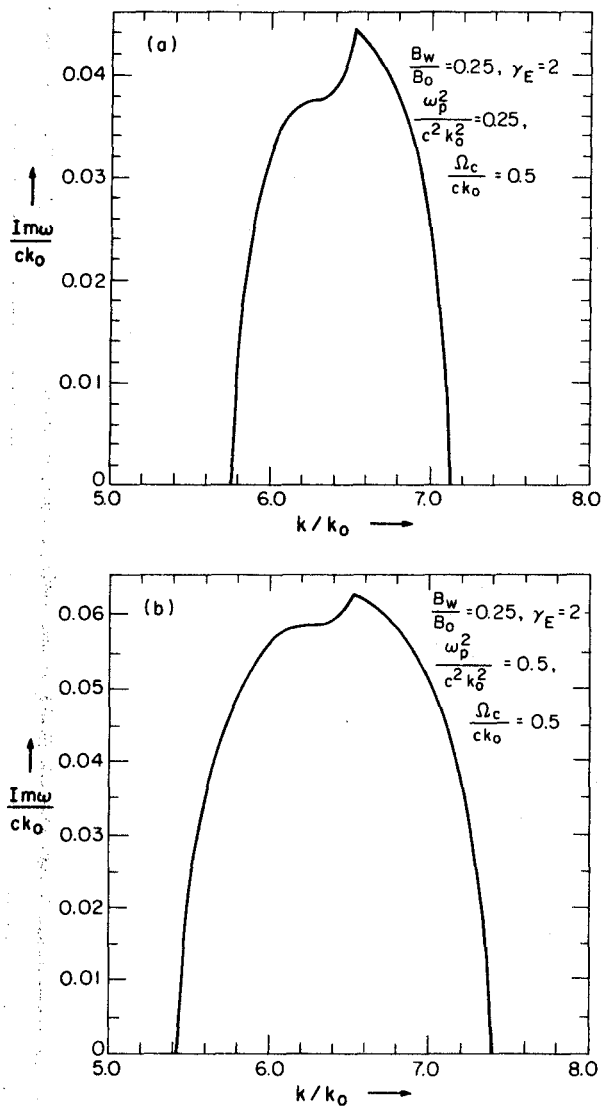

FIG. 3. Plot of the normalized growth rate $\mathrm{Im}\,\omega/ck_0$ vs k/k_0 obtained numerically from Eq. (50) for the upshifted unstable mode with $\omega \simeq (k + k_0)V_E$. Parameters correspond to $\gamma_E = 2$, $B_w/B_0 = 0.25$, $\Omega_c/ck_0 = 0.5$, and (a) $\omega_p^2/c^2k_0^2 = 0.25$ and (b) $\omega_p^2/c^2k_0^2 = 0.5$.

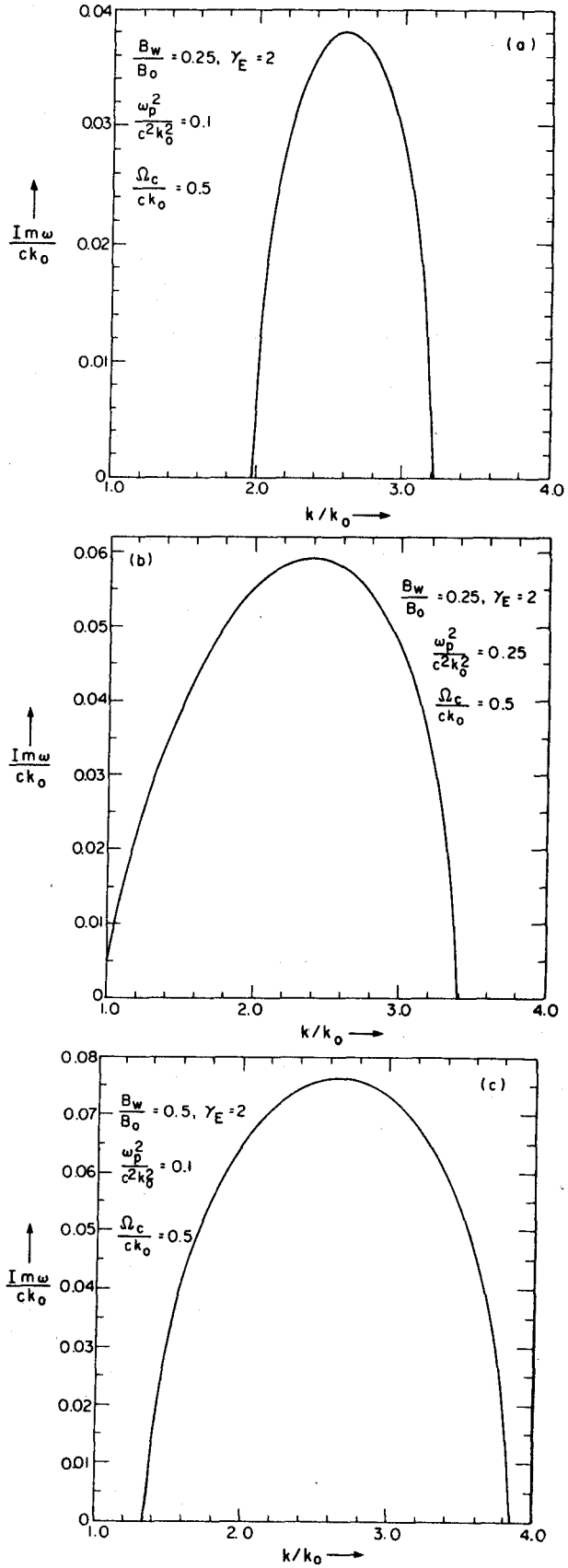

FIG. 4. Plot of the normalized growth rate $\mathrm{Im}\,\omega/ck_0$ vs k/k_0 obtained numerically from Eq. (50) for the unstable dowshifted cyclotron branch with $\omega - (k + k_0)V_E \simeq -\Omega_c/\gamma_E$. Parameters correspond to $\gamma_E = 2$ and $\Omega_c/ck_0 = 0.5$ and (a) $B_w/B_0 = 0.25$ and $\omega_p^2/c^2k_0^2 = 0.1$, (b) $B_w/B_0 = 0.25$ and $\omega_p^2/c^2k_0^2 = 0.25$, and (c) $B_w/B_0 = 0.5$ and $\omega_p^2/c^2k_0^2 = 0.1$.

V. CONCLUSIONS

The present theoretical analysis of the cross-field FEL instability is based on the macroscopic, relativistic cold-fluid equations for the electrons [Eqs. (5) and (6)] coupled with Maxwell's equations for the fields [Eqs. (8) and (9)], where it is assumed that the wave perturbations have ordinary-mode polarization with $\delta\mathbf{E} = \delta E_z \hat{\mathbf{e}}_z$ and $\delta\mathbf{B} = \delta B_x \hat{\mathbf{e}}_x + \delta B_y \hat{\mathbf{e}}_y$. The electron beam density is assumed to be sufficiently low that equilibrium self-field effects are negligibly small and the Compton-regime approximation is valid with negligibly small perturbation in electrostatic potential ($\delta\phi \simeq 0$). In Sec. III, the equilibrium flow was examined in the limit of small wiggler amplitude $e^2 B_w^2/m^2c^4k_0^2 \ll 1$ [Eq. (25)] and weak spatial variation in electron energy $\gamma_0(x)mc^2$ across the anode–cathode gap [Eq. (26)]. The average equilibrium electron flow is then approximately $V_y^0 = V_E = -cE_0/B_0$ [Eq. (27)] with a small wiggler-induced modulation of the axial flow velocity $V_z^0 = -(eB_w/\hat{\gamma}mck_0)\cos k_0 y$. For ordinary-mode perturbations with $\partial/\partial z = 0$, detailed stability properties were determined from the coupled eigenvalue equations (38)–(42) in the limit of weak transverse spatial variations with $|\partial/\partial x| \ll |\partial/\partial y|$. For small wiggler amplitude and beam density, the resulting matrix dispersion equation (47) is approximated by the diagonal terms which give the dispersion relation in Eq. (50). Analytic and numerical estimates (Sec. IV) of the FEL growth rate obtained from Eq. (50) show that the upshifted resonance term proportional to $[\omega - (k + k_0)V_E]^{-1}$ in Eq. (50) leads to instability with characteristic maximum growth rate [Eq. (56)]

$$\mathrm{Im}(\delta\omega) = (\omega_p/2\sqrt{2})(\Omega_w/ck_0),$$

and emission frequency [Eq. (54)]

$$\omega_r = (1 + \beta_E)\gamma_E^2 k_0 V_E,$$

where $\beta_E = V_E/C$. Depending on the size of Ω_w/ck_0, Eq. (56) can correspond to relatively short exponentiation times in units of ω_p^{-1}.

ACKNOWLEDGMENTS

It is a pleasure to acknowledge the benefit of useful discussions with Richard Aamodt and George Bekefi.

This work was supported in part by the Office of Naval Research and in part by the Air Force Aeronautical Systems Division.

[1] V. P. Sukhatme and P. A. Wolff, J. Appl. Phys. **44**, 2331 (1973).
[2] W. B. Colson, Phys. Lett. **59A**, 187 (1976).
[3] T. Kwan, J. M. Dawson, and A. T. Lin, Phys. Fluids **20**, 581 (1977).
[4] N. M. Kroll and W. A. McMullin, Phys. Rev. A **17**, 300 (1978).
[5] P. Sprangle and R. A. Smith, Phys. Rev. A **21**, 293 (1980).
[6] R. C. Davidson and H. Uhm, Phys. Fluids **23**, 2076 (1980).
[7] H. S. Uhm and R. C. Davidson, Phys. Fluids **24**, 1541 (1981).
[8] W. B. Colson, IEEE J. Quant. Electron. **QE17**, 1417 (1981).
[9] W. A. McMullin and G. Bekefi, Appl. Phys. Lett. **39**, 845 (1981).
[10] W. A. McMullin and G. Bekefi, Phys. Rev. A **25**, 1826 (1982).
[11] R. C. Davidson and W. A. McMullin, Phys. Rev. A **26**, 1997 (1982).
[12] R. C. Davidson and W. A. McMullin, Phys. Fluids **26**, 840 (1983).
[13] L. R. Elias, W. M. Fairbank, J. M. J. Madey, H. A. Schwettman, and T. I. Smith, Phys. Rev. Lett. **36**, 717 (1976).
[14] D. A. G. Deacon, L. R. Elias, J. M. J. Madey, G. J. Ramian, H. A. Schwettman, and T. I. Smith, Phys. Rev. Lett. **38**, 892 (1977).
[15] D. B. McDermott, T. C. Marshall, S. P. Schlesinger, R. K. Parker, and V. L. Granatstein, Phys. Rev. Lett. **41**, 1368 (1978).
[16] S. Benson, D. A. G. Deacon, J. N. Eckstein, J. M. J. Madey, K. Robinson, T. I. Smith, and R. Taber, Phys. Rev. Lett. **48**, 235 (1982).
[17] R. K. Parker, R. H. Jackson, S. H. Gold, H. P. Freund, V. L. Granatstein, P. C. Efthimion, M. Herndon, and A. K. Kinkead, Phys. Rev. Lett. **48**, 238 (1982).
[18] A. N. Didenko, A. R. Borisov, G. R. Fomenko, A. V. Kosevnikov, G. V. Melnikov, Yu G. Stein, and A. G. Zerlitsin, IEEE Trans. Nucl. Sci. **28**, 3169 (1981).
[19] A. Grossman, T. C. Marshall, and S. P. Schlesinger, Phys. Fluids **26**, 337 (1983).
[20] A. Grossman and T. C. Marshall, IEEE J. Quant. Electron **QE-19**, 334 (1983).
[21] G. Bekefi, Appl. Phys. Lett. **40**, 578 (1982).